IEEE Access
Multidisciplinary | Rapid Review | Open Access Journal

Received 7 February 2023, accepted 25 February 2023, date of publication 3 March 2023, date of current version 9 March 2023.

Digital Object Identifier 10.1109/ACCESS.2023.3252371

RESEARCH ARTICLE

Increasing Unbalanced Distribution Network's Hosting Capacity for Distributed Energy Resources by Voltage Regulators

SINA TOGHRANEGAR[1], ABBAS RABIEE[1], (Senior Member, IEEE), AND SEYED MASOUD MOHSENI-BONAB[2], (Senior Member, IEEE)
[1]Department of Electrical Engineering, University of Zanjan, Zanjan 45371-38111, Iran
[2]Hydro-Québec Research Institute (IREQ), Digital Systems, Varennes, QC J3X 1S1, Canada

Corresponding author: Seyed Masoud Mohseni-Bonab (S.m.mohsenibonab@ieee.org)

ABSTRACT Renewable energy sources (RESs) are becoming promising nowadays. Deploying distributed energy resources (DERs) is thus increasing accordingly, but the intermittent nature associated with RES remains a significant challenge. Also, the distribution grid faces technological difficulties with the large-scale integration of PV generations and EV charging loads. This paper suggests a strategy for a novel optimal voltage regulator (VR) placement model associated with the optimal placement of electric vehicle chargers (EVCs) and photovoltaic (PV) cells. Also, VRs' reference voltages are determined optimally to enhance the hosting capacity (HC) of three-phase unbalanced distribution feeders for large-scale residential/public EVCs and PVs. Two scenarios are defined to study the impact of VRs on the network's HC for DERs, namely with and without VRs in the real three-phase unbalanced feeder. The developed model determines the optimal placement of VRs and their reference voltages linked with EVCs and PVs penetration. Time-Varying Acceleration Coefficients Iteration Particle Swarm Optimization (TVAC-IPSO) algorithm has been implemented to improve the real three-phase unbalanced distribution feeder's HC for DERs. The efficiency of the proposed model and the solution method is validated on the modified IEEE 37-node medium voltage (MV) radial distribution network connected to 35 low voltage (LV) distribution feeders. The obtained results represent that installing a proper number of VRs will increase the network's HC for DERs.

INDEX TERMS Electric vehicle (EV), particle swarm optimization (PSO), photovoltaic (PV), unbalanced distribution network, voltage regulator (VR).

NOMENCLATURE

The notations and symbols used throughout the paper are stated in this section.

A. ABBREVIATIONS

CO2	Carbon Dioxide.
DER	Distributed Energy Resource.
DG	Distributed Generation.
DSO	Distribution System Operator.
EMS	Energy Management System.
ESS	Energy Storage System.
EV	Electric Vehicle.
EVC	EV Charger.
GA	Genetic Algorithm.
HBMO	Honeybee-mating optimization.
HC	Hosting Capacity.
LV	Low Voltage.
MA	Memetic Algorithm.
MV	Medium Voltage.
PC	Power Conversion.
PSO	Particle Swarm Optimization.
PV	Photovoltaic.
RES	Renewable energy source.
ST2	Standard Type-2.
TLBO	Teaching-learning based optimization.

The associate editor coordinating the review of this manuscript and approving it for publication was Miadreza Shafie-Khah.

$TVAC-IPSO$	Time Varying Acceleration Coefficients Iteration Particle Swarm Optimization.
VR	Voltage Regulator.

B. SETS/INDICES

b	Index for electrical network buses.
f	Index for iteration of power flow.
k	Index for EVC type (residential or public).
s	Index for phases (i.e. A, B, and C).
t	Index for operation intervals.

C. VARIABLES

$a_{R\_ab}, a_{R\_bc}, a_{R\_ca}$	Voltage regulator effective turn ratios.
$I^s_{b,t}$	Current flowing out of bus b at phase s and time t.
$I^s_{bc,t}$	Current flowing between bus b and c at phase s and time t.
I_{PC}	Compensation current of power conversion element.
I_{AB}, I_{BC}, I_{CA}	Currents of the source side of the voltage regulator.
I_{ab}, I_{bc}, I_{ca}	Currents of the load side of the voltage regulator.
$PEV^{s,k}_{b,t}$	Active power consumption of type k of EVC at bus b, phase s, and time t.
$PG^s_{b,t}$	Active power generation at bus b, phase s, and time t.
$PGslack^s_t$	Active power generation at slack bus at phase s and time t.
$PL^s_{b,t}$	Active power demand at bus b, phase s, and time t.
$PPV^s_{b,t}$	Active power generation by PV at bus b, phase s, and time t.
$QEV^{s,k}_{b,t}$	Reactive power generated or consumed by type k of EVC at bus b, phase s, and time t.
$QG^s_{b,t}$	Reactive power generation at bus b, phase s, and time t.
$QGslack^s_t$	Reactive power generation at slack bus at phase s and time t.
$QL^s_{b,t}$	Reactive power demand at bus b, phase s, and time t.
$QPV^s_{b,t}$	Reactive power generated or consumed by PV at bus b, phase s, and time t.
V_f	System voltage vector at f-th iteration of power flow done by OpenDSS.
$V^s_{b,t}$	Voltage at bus b, phase s, and time t.
V_{AB}, V_{BC}, V_{CA}	Three-phase voltages of the source side of the voltage regulator.
V_{ab}, V_{bc}, V_{ca}	Three-phase voltages of the load side of the voltage regulator.
Y_{system}	Admittance matrix of system.

D. PARAMETERS

$I_{bc,max}$	Thermal limit of lines between buses b and c.
N_1	Number of turns on the shunt winding.
N_2	Number of turns on the series winding.
$Pdemand^s_{b,t}$	Active power demand of the network at bus b, phase s, and time t.
$Qdemand^s_{b,t}$	Reactive power demand of the network at bus b, phase s, and time t.
$QEV^{s,k}_{b,max}$	Maximum reactive power capacity of EVCs' inverters.
$QEV^{s,k}_{b,min}$	Minimum reactive power capacity of EVCs' inverters.
$QPV^s_{b,max}$	Maximum reactive power capacity of PVs' inverters.
$QPV^s_{b,min}$	Minimum reactive power capacity of PVs' inverters.
$SGslack_{max}$	Maximum apparent power generation at slack bus.
V_{min}	Minimum voltage limit.
V_{max}	Maximum voltage limit.

I. INTRODUCTION

A. BACKGROUND AND LITERATURE REVIEW

As a result of growing concerns about the emissions by thermal power plants, RESs have turned out to be the best alternative to supply electricity demand. Nowadays, all means of transportation are responsible for considerable CO2 emissions. All the endeavors will improve climate and air quality, and in this path, the modes of transportation's impact are crucial [1]. Moreover, DERs such as PV and EVCs can be the best solution to decarbonize the cities [2]. Therefore, the utilization of PV systems and electric vehicles (EVs) has increased these years.

Nevertheless, using PV systems has caused some adverse effects on the power systems. Notably, integrating the PV systems into the grid has caused voltage violations [3], [4]. On the other hand, excess EVCs can lead to increased power flow in power cables, transformer overloading, voltage drop, and voltage unbalance [5].

There is a specific HC for each generation type, such as PVs, and each load type, such as EVCs. The HC is defined as the amount of generation or load that can be integrated into the power grid without endangering the network's reliability and power quality [6]. Increasing networks' HC for PVs and EVCs has recently been a popular topic. Study in [7] presents a novel combination of teaching-learning based optimization (TLBO) and honeybee-mating optimization (HBMO) algorithms to solve the placement of DERs on a distribution system containing previously installed DERs and take their HC into account. The proposed combination of the HBMO and TLBO algorithms improves robustness and convergence speed. The objective functions are cost reduction, technical losses, and voltage variation reduction. The findings

demonstrate that the suggested algorithm achieves the optimal solution with improved precision and computational speed. In [8], carbon-efficient virtual machine placement was addressed. Solar energy was also explored as a source of energy supply to lower energy and carbon consumption expenses. A multi-objective virtual machine placement was proposed to minimize energy costs and scheduling. This problem was solved on a big scale using a modified Memetic Algorithm (MA). Then, the performance of the suggested method was compared to that of a baseline algorithm, such as the Genetic Algorithm (GA), and cutting-edge algorithms. In [9], a two-stage approach to assessing and improving the HC limit of uncertain RESs, such as PVs, in the electricity network. In addition, several uncertainty scenarios are utilized to illustrate the effect of RESs and load uncertainty on HC limit. The proposed technique achieves up to 77.8% RESs integration for the tested systems from total load demand. In [10], a co-optimization generation and transmission planning methodology was suggested in this research to maximize HC for large-scale PVs. This model's solution also provides the ideal PV size, location, and required PV energy curtailment. In [11], a novel techno-economic methodology for an off-grid remote industrial microgrid was presented to improve PV's HC by including battery energy storage while considering grid disturbance and recovery scenarios. The research discovered that integrating battery energy storage systems into the microgrid increased the system's PV hosting capacity. The research studied in [12] suggests a method for increasing the HC of LV distribution network for PV. Probabilistic and deterministic techniques were used to evaluate the influence of the stochastic effect of PV installations on voltage and ampacity, which directly affect the HC of LV distribution networks for PV. Coordinated voltage control was used in conjunction with an on-load tap changing transformer and PV inverter reactive power compensation and active power curtailment. The study in [13] investigated the impact of various connection standards on HC for PVs and their applicability in LV distribution networks. Smart inverters with differing Volt-VAr and Volt-Watt control functions were modeled. Smart inverter functions with higher reactive power consumption significantly increased the HC. In [14], a real-time optimal power flow approach for coordinated control of distributed PV inverters presented a unique distributed energy resource management system solution. The proposed approach can improve the distribution grids' HC for PVs. A single-phase EV charging coordination technique with a three-phase network supply was proposed in [15]. Chargers link EVs to the feeder's less-loaded phase at the start of charging. Results show that the network's imbalance was reduced, and HC for EVs was raised.

The study [16] aims to give a combined PV-EV grid integration and HC assessment for a residential LV distribution grid with various energy management system (EMS) scenarios. The results demonstrate that EVs smart charging can greatly enhance HC for EVs and modestly improve HC for PVs. In [17], an approach was proposed for estimating the HC of renewable-based distributed generation (DG) and EV in electric distribution systems from the perspective of the distribution system operator (DSO). In part of the analysis, the penetration level of EVs was gradually increased to evaluate its impacts on the HC for DGs. Operational resources such as generation curtailment and EV charging coordination systems were adjusted to ensure electric distribution system operation while avoiding technical limit violations and decreasing energy losses to maximize the network's HC for DGs and EVs. The study presented in [18] examines how a model-predictive-control-based energy management system can increase the HC for PVs and EVs in a standalone microgrid with an energy storage system (ESS).

TABLE 1. Summary of the existing literature.

References	PV	EV	VR	Large-scale integraion of DERs		Unbalanced networks
[7]						
[8]	✓			✓		
[9]	✓					
[10]	✓			✓		
[11]	✓			✓		
[12]	✓			✓	✓	Lotus Grove's feeder, Sri Lanka
[13]	✓					
[14]	✓			✓	✓	IEEE 13-bus
[15]		✓		✓	✓	Three real UK North West's electricity distribution networks
[16]	✓	✓		✓	✓	IEEE European LV Test Feeder with 55 households
[17]	✓	✓		✓		
[18]	✓	✓				
This paper	✓	✓	✓	✓	✓	IEEE 37 bus MV network with 35 LV feeders

A summary of the existing research performed recently is given in Table 1.

B. CONTRIBUTIONS

Connecting large-scale EVCs demand blocks to the grid will significantly increase total electricity demand due to the large electricity consumption of EVs. However, the grid can face severe technical problems such as reverse power flows, voltage violations, and line congestion. Also, in all the scenarios that have been predicted for energy transition, RESs play a crucial role. Among the RESs, PV is the most prominent type at the distribution system level due to its scalability and installation convenience. Optimal VR placement in a

distribution network is an effective strategy to enhance the HC for DERs since VR can regulate voltage. The VR contains an auto-transformer and is identified as a step voltage changer. The voltage variations are caused by changes in the number of tap changers in the auto-transformer's winding. Moreover, VRs can control voltage fluctuations and violations that connect PVs and EVCs to the distribution grids. So by installing VRs in distribution feeders and their optimal allocation and voltage settings, the feeder's HC for large-scale PVs and EVCs can be increased by alleviating voltage violations as well as reducing voltage unbalance. Hence, this paper studies the optimal allocation of the PVs and EVCs in real three-phase unbalanced LV distribution grids and their generated or consumed reactive power. To maximize the LV network's HC for PVs and EVCs, VRs are optimally allocated in the primary MV grid to alleviate voltage unbalance in both MV and LV levels. Thus, two main scenarios have been studied, namely:

- Scenario-I: maximization of LV distribution grid's HC for EVCs and PVs, without considering any VR installation.
- Scenario-II: maximization of LV distribution grid's HC for EVCs and PVs, with considering VR installation in MV level.

II. METHODOLOGY

A. ASSUMPTIONS

Considering the growing number of EVs, EVCs' inherent influences are increasing significantly on the electricity grids and electricity markets. The quantity and types of EVs, energy usage, and location are the most significant influencing factors. EVC technology can minimize the potential impacts of EVs' demand on the electricity grid and the electricity markets. Solar power generation installed in residential areas uses inverter technology. Managing the balance of active and reactive power in a PV inverter improves the voltage profile, making it easier to increase the HC while avoiding the need for grid reinforcements. In this section, an optimization model is proposed to optimally allocate the EVCs, PVs, and VRs in three-phase unbalanced MV and LV distribution feeders. The proposed model has the following features:

- Considering profiles of load demand, public and residential EVCs demand, and PVs generation.
- Considering power factor for the mentioned DERs.
- Optimal allocation of VRs in the MV distribution grid in terms of their location and corresponding reference voltages.
- Optimal allocation for PVs and EVCs in the LV distribution grid and their generated or consumed reactive power.
- The MV and LV distribution grid technical constraints such as three-phase power flow, current, and voltage limits are satisfied in the entire operational horizon.

B. MATHEMATICAL FORMULATION

1) OBJECTIVE FUNCTION

The aim is to maximize the network's HC for EVCs' energy demand and PVs' energy generation, as follows.

$$\max \quad HC = \sum_{b,s,t,k} PEV^{s,k}_{b,t} + \sum_{b,s,t} PPV^{s}_{b,t}$$
$$Subject\ \ to: (2)\ to\ (12) \tag{1}$$

where $PEV^{s,k}_{b,t}$ is active power consumption of type k of EVC, and $PPV^{s}_{b,t}$ is active power generation by PV at bus b, phase s, and time t.

2) PROBLEM CONSTRAINTS

a: POWER BALANCE CONSTRAINT

The power balance equations can be defined as follows [19].

$$PG^{s}_{b,t} - PL^{s}_{b,t} = \Re\{V^{s}_{b,t} \cdot (I^{s}_{b,t})^{*}\} \tag{2}$$
$$QG^{s}_{b,t} - QL^{s}_{b,t} = \Im\{V^{s}_{b,t} \cdot (I^{s}_{b,t})^{*}\} \tag{3}$$

where $\Re\{\cdot\}$ and $\Im\{\cdot\}$ represent the real and imaginary components of a complex number, respectively. $PG^{s}_{b,t}$ and $QG^{s}_{b,t}$ represent the active and reactive power generation, and $PL^{s}_{b,t}$ and $QL^{s}_{b,t}$ denote the active and reactive power demand at bus b, phase s, and time t. $V^{s}_{b,t}$ is voltage at bus b, phase s, and time t, while $I^{s}_{b,t}$ is current flowing out of bus b at phase s and time t. Additionally, $PG^{s}_{b,t}$, $PL^{s}_{b,t}$, $QG^{s}_{b,t}$, and $QL^{s}_{b,t}$ can be defined as follows.

$$PG^{s}_{b,t} = PGslack^{s}_{t} + PPV^{s}_{b,t} \tag{4}$$
$$PL^{s}_{b,t} = Pdemand^{s}_{b,t} + PEV^{s,k}_{b,t} \tag{5}$$
$$QG^{s}_{b,t} = QGslack^{s}_{t} + QPV^{s}_{b,t} \tag{6}$$
$$QL^{s}_{b,t} = Qdemand^{s}_{b,t} + QEV^{s,k}_{b,t} \tag{7}$$

where $PGslack^{s}_{t}$ and $QGslack^{s}_{t}$ represent active and reactive power generation at the slack bus at phase s and time t, respectively. It should be noted that the $PGslack^{s}_{t}$ and $QGslack^{s}_{t}$ are the variables that only have values at the slack bus. In addition, $QPV^{s}_{b,t}$ represents reactive power generated or consumed by PV, $QEV^{s,k}_{b,t}$ is reactive power generated or consumed by type k of EVC at bus b, phase s, and time t. $Pdemand^{s}_{b,t}$ is the active power demand of the network, whereas $Qdemand^{s}_{b,t}$ is the reactive power demand of the network at bus b, phase s, and time t.

b: SLACK BUS POWER RATING CONSTRAINT

The slack bus power rating constraint indicates the rating of the primary transformer feeding the feeder.

$$\left(PGslack^{s}_{t}\right)^{2} + \left(QGslack^{s}_{t}\right)^{2} \leq (SGslack_{max})^{2} \tag{8}$$

where $SGslack_{max}$ is the maximum apparent power generation at the slack bus.

c: VOLTAGE CONSTRAINT

The magnitude of the steady-state voltage at each node must obey the voltage limits defined in constraint (9). Voltage

limits at each node should be ±10% of rated voltage.

$$V_{min} \leq \left|V^s_{b,t}\right| \leq V_{max} \tag{9}$$

d: LINE CURRENT CONSTRAINT

The current flowing between buses b and c at phase s and time t, $I^s_{bc,t}$, should not exceed the thermal limit, i.e., $I_{bc,max}$, as per constraint (10):

$$I^s_{bc,t} \leq I_{bc,max} \tag{10}$$

e: REACTIVE POWER CAPABILITY OF DERs

The following limits are considered for the reactive power capabilities of DERs.

$$QPV^s_{b,min} \leq QPV^s_{b,t} \leq QPV^s_{b,max} \tag{11}$$

$$QEV^{s,k}_{b,min} \leq QEV^{s,k}_{b,t} \leq QEV^{s,k}_{b,max} \tag{12}$$

where $QPV^s_{b,min}$, $QEV^{s,k}_{b,min}$, $QPV^s_{b,max}$, and $QEV^{s,k}_{b,max}$ are minimum and maximum reactive power capacity of DERs' inverters.

C. UNBALANCED THREE-PHASE POWER FLOW

The unbalanced three-phase power flow is modeled as follows.

$$V_{f+1} = [Y_{system}]^{-1} I_{PC}(V_f)$$
$$f = 0, 1, 2, \ldots, until\ converged \tag{13}$$

The equation is derived from the circuit solution technique in the EPRI OpenDSS [20], which is written as a simple "fixed-point iterative" method. The process of power flow using OpenDSS starts with building the admittance matrix of the system (i.e., Y_{system}). The software initiates the process with a guess at system voltage vector, V_0, and computes the compensation currents from each power conversion (PC) element to put values in the I_{PC} vector. The new estimates of voltage, i.e., V_{f+1}, are calculated in (13) by using a sparse matrix solver. This process will be repeated until a convergence criterion is met. This method can handle extensive load models in which I_{PC} can be expressed as a consistent function of V_f.

D. VR MODEL

In this paper, three single-phase regulators in a closed delta connection have been considered [21]. Each regulator has an effective turn ratio (a_{R_ab}, a_{R_bc}, and a_{R_ca}), which can be assigned to different values. The values can be $1 + 0.00625\times$ steps, which steps are between -16 to 16 as integers. The positions of the VRs in Fig. 1 are in raised positions ($1 + 0.00625\times$ step, which step $\in [1, 16]$ as integers). In Fig. 1-(a), closed delta-connected regulators with voltages have been shown.

The relationships of the voltages and currents between the source side and load side are required. Starting with the line-to-line voltage between phases A and B on the source side, Kirchhoff's Voltage Law is initially applied around a closed loop. The V_{AB} can be written as follows.

$$V_{AB} = V_{Aa} + V_{Ab} - V_{Bb} \tag{14}$$

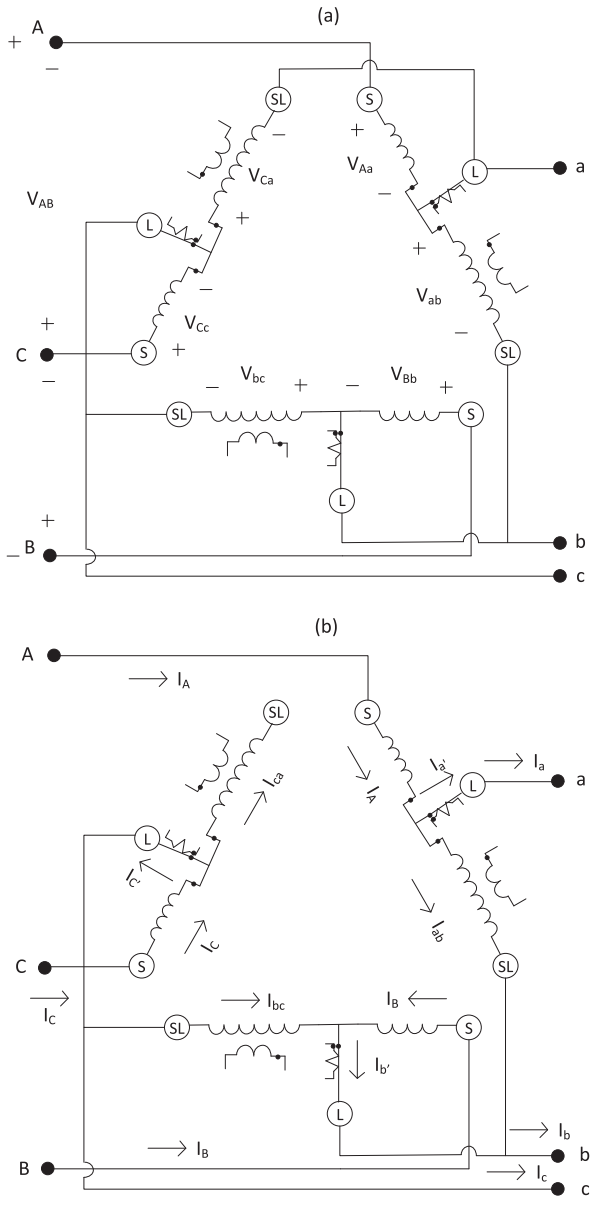

FIGURE 1. Three single-phase VRs in a closed delta connection with, (a): voltages, (b): currents.

where V_{Aa} and V_{Bb} can be written:

$$V_{Aa} = -\frac{N_2}{N_1}.V_{ab} \tag{15}$$

$$V_{Bb} = -\frac{N_2}{N_1}.V_{bc} \tag{16}$$

Then by substituting equations (15) and (16) with equation (14) and simplifying the resulting equation:

$$V_{AB} = (1 - \frac{N_2}{N_1}).V_{ab} + \frac{N_2}{N_1}.V_{bc}$$
$$= a_{R\_ab}.V_{ab} + (1 - a_{R\_bc}).V_{bc} \tag{17}$$

In order to find the relationships between the other line-to-line voltages, the same technique can be followed. The

concluding three-phase equation is:

$$\begin{bmatrix} V_{AB} \\ V_{BC} \\ V_{CA} \end{bmatrix} = \begin{bmatrix} a_{R\_ab} & 1-a_{R\_bc} & 0 \\ 0 & a_{R\_bc} & 1-a_{R\_ca} \\ 1-a_{R\_ab} & 0 & a_{R\_ca} \end{bmatrix} . \begin{bmatrix} V_{ab} \\ V_{bc} \\ V_{ca} \end{bmatrix} \tag{18}$$

The (18) expresses the relationship between the source and load side three-phase voltages of the VR installed in the grid.

Figure 1-(b) displays the closed delta–delta connection with the currents. The relationship between source and load line currents at terminal a can be written as follows.

$$I_a = I_{a'} + I_{ca} = I_A - I_{ab} + I_{ca} \tag{19}$$

$$I_{ab} = \frac{N_2}{N_1}.I_A \tag{20}$$

$$I_{ca} = \frac{N_2}{N_1}.I_C \tag{21}$$

where by substituting equations (20) and (21) in equation (19), the I_a can be written as follows.

$$I_a = (1 - \frac{N_2}{N_1}).I_A + \frac{N_2}{N_1}.I_C = a_{R\_ab}.I_A + (1 - a_{R\_ca}).I_C \tag{22}$$

The similar approach can be applied to the remaining two load side terminals. The consequent three-phase equation is as follows.

$$\begin{bmatrix} I_a \\ I_b \\ I_c \end{bmatrix} = \begin{bmatrix} a_{R\_ab} & 0 & 1-a_{R\_ca} \\ 1-a_{R\_ab} & a_{R\_bc} & 0 \\ 0 & 1-a_{R\_bc} & a_{R\_ca} \end{bmatrix} . \begin{bmatrix} I_A \\ I_B \\ I_C \end{bmatrix} \tag{23}$$

E. OPTIMIZATION MODEL FOR DIFFERENT SCENARIOS

- Scenario-I
  In this scenario, the model aims to maximize the existing network's HC for DERs by finding their optimal location and their generated or consumed reactive power without installing any VRs. The capability of the distribution network for hosting DERs is limited by power flow constraints and operational limits such as voltage/current limits. Hence, the objective function (1) will be maximized in this scenario without using any VR.
- Scenario-II
  In this scenario, the model aims to maximize the network's HC for mentioned DERs by finding their optimal location and their generated or consumed reactive power with installations of the VRs. The optimal number of the VRs will be analyzed in several test cases by finding the VRs' optimal location and optimal reference voltages. Therefore, by considering all the problem constraints, the objective function (1) will be maximized by installing VRs.

An overview of the optimization framework and its properties implemented in this study is demonstrated in Fig. 2.

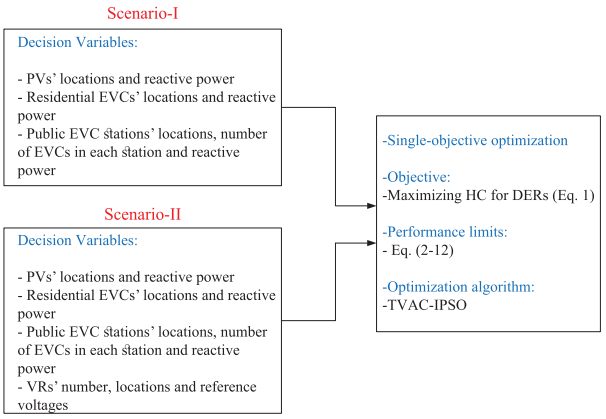

FIGURE 2. Proposed optimization framework.

F. TIME VARYING ACCELERATION COEFFICIENTS ITERATION PARTICLE SWARM OPTIMIZATION

The optimization model proposed in this study is essentially a combinational optimization problem in terms of optimal allocation of DERs and their generated or consumed reactive power, VRs, and reference voltages. In addition, as the unbalanced three-phase AC power flow model is included, the proposed model is a mixed integer nonlinear programming (MINLP) model. Typical gradient-based methods have trouble solving an MINLP model that is as complicated as this, but metaheuristic methods can easily handle it.

1) CLASSIC PARTICLE SWARM OPTIMIZATION

PSO is a population-based stochastic search algorithm that has become very popular for solving optimization problems. Kennedy and Eberhart developed this intelligent stochastic search algorithm in 1995 for the first time [22]. PSO begins with a chosen number of randomly initialized particles in an N-dimensional solution space. A particle k at iteration $iter$ has a position vector X_k^{iter} and a velocity vector V_k^{iter}. The best solution achieved by k_{th} particle until the existing iteration ($iter$) can be shown as $P_{best_k}^{iter}$. Among the whole particles, the best $P_{best_k}^{iter}$ can be denoted as global best g_{best}^{iter}. Then, the velocity and position of every particle will be updated using the following equations.

$$v_{kn}^{iter+1} = \omega \times v_{kn}^{iter} + C_1 \times r_1^n \times (p_{best_{kn}}^{iter} - x_{kn}^{iter}) + C_2 \times r_2^n \times (g_{best}^{iter} - x_{kn}^{iter}) \tag{24}$$

$$x_{kn}^{iter+1} = x_{kn}^{iter} + v_{kn}^{iter+1} \tag{25}$$

where ω is inertia weight, which can be calculated using (26), r_1^n and r_2^n are two autonomously generated random numbers between 0 and 1. C_1 and C_2 are cognitive and social component acceleration coefficients, respectively.

$$\omega = \omega_{max} - \frac{\omega_{max} - \omega_{min}}{iter_{max}} \times iter \tag{26}$$

where ω_{min} and ω_{max} are initial weight and final weight, respectively. $iter_{max}$ is the maximum iteration number.

2) TVAC-IPSO

A new index named iteration best is added to (24) to improve the performance of PSO. This method is known as Iteration PSO (IPSO) [27], [28], [29]. Thus, the velocity updating formula considering iteration best will be as follows.

$$v_{kn}^{iter+1} = \omega \times v_{kn}^{iter} + C_1 \times r_1^n \times (p_{best_{kn}}^{iter} - x_{kn}^{iter}) + C_2 \times r_2^n \times (g_{best}^{iter} - x_{kn}^{iter}) + C_3 \times r_3^n \times (I_{best}^{iter} - x_{kn}^{iter}) \quad (27)$$

I_{best}^{iter} is the best solution that any particle has found in iteration $iter$. C_3 is the weighting factor of stochastic acceleration. r_3^n is a random number in the range of [0,1]. In the TVAC-IPSO algorithm, the following equations will update the acceleration coefficients.

$$C_1 = C_{1i} + \frac{C_{1f} - C_{1i}}{iter_{max}} \times iter \quad (28)$$

$$C_2 = C_{2i} + \frac{C_{2f} - C_{2i}}{iter_{max}} \times iter \quad (29)$$

where C_{1i}, C_{1f}, C_{2i} and C_{2f} are initial and final values of cognitive and social components acceleration factors, respectively. Moreover, C_3 will be updated as follows:

$$C_3 = C_1 \times (1 - e^{(-C_2 \times iter)}) \quad (30)$$

III. CASE STUDIES AND NUMERICAL RESULTS

A. CASE STUDIES

In order to determine the optimal locations of PVs, EVCs, and their generated or consumed reactive power, VRs, and their reference voltages, numerical studies are done on the modified IEEE 37-bus MV distribution network using OpenDSS [31]. The single-line diagram of this system is depicted in Fig. 3. Also, modified 35 LV distribution grids with 107 buses and 55 load points for each grid, derived from [32], have been connected to the 35 buses of the MV distribution grid. The single-line diagram of one of the LV grids is depicted in Fig. 4.

B. TVAC-IPSO PARAMETER SELECTION

The selection of proper values for the algorithm plays a crucial role in both the quality of the solution and the speed of the algorithm's convergence. The optimal value for the population size is chosen to be 50. Also, the proper maximum iteration number is chosen to be 100. The effect of the initial and final values of cognitive and social component acceleration factors on solution performance is studied by varying their values for the above optimal population size values and maximum iteration number. The resultant optimal parameters for the proposed algorithm based on the above analysis are as follows: $\omega_{max} = 0.9$, $\omega_{min} = 0.4$, $C_{1i} = 1.75$, $C_{1f} = C_{2i} = 0.5$, $C_{2f} = 2$.

C. DATA

Two types of EV chargers are considered here (i.e., residential and public chargers). The residential EVC type is Standard Type-2 (ST2), whereas the fast chargers (AC43, CCS, and CHAdeMO) are commonly used in public locations because of their fast charging capabilities. It is assumed that the public EVCs' each charge point has a maximum capacity of 4 × 22 kW. Furthermore, each point of the residential EVCs has a single-phase connection with a capacity of 3.7 kW.

The demand profiles of residential and public EVCs are depicted in Fig. 5. These EVCs demand profiles are driven from [33] and [34], respectively. These profiles, obtained through an extensive data set of EV charge events from 2017 to 2019 in the UK and Ireland, show the average daily usage of each EVC. It can be observed from Fig. 5-(a)

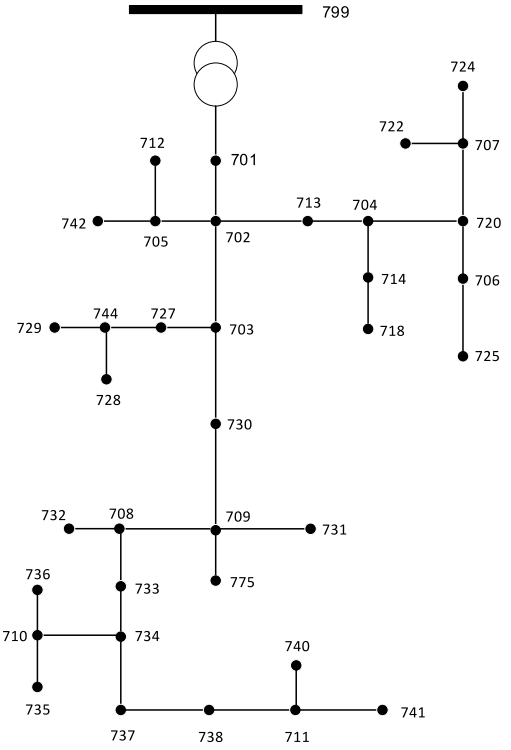

FIGURE 3. Single-line diagram of IEEE 37-bus MV distribution network.

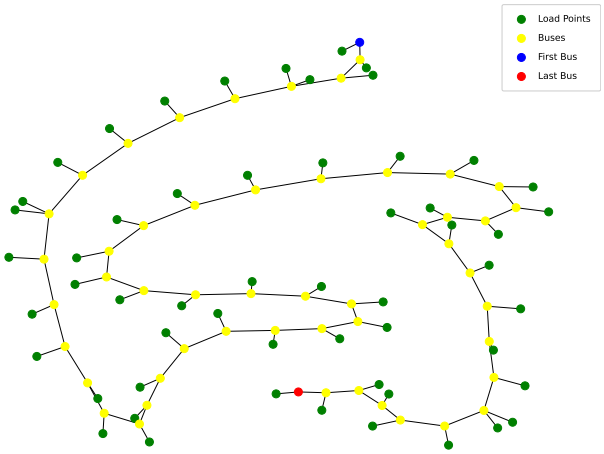

FIGURE 4. Single-line diagram of the LV grid.

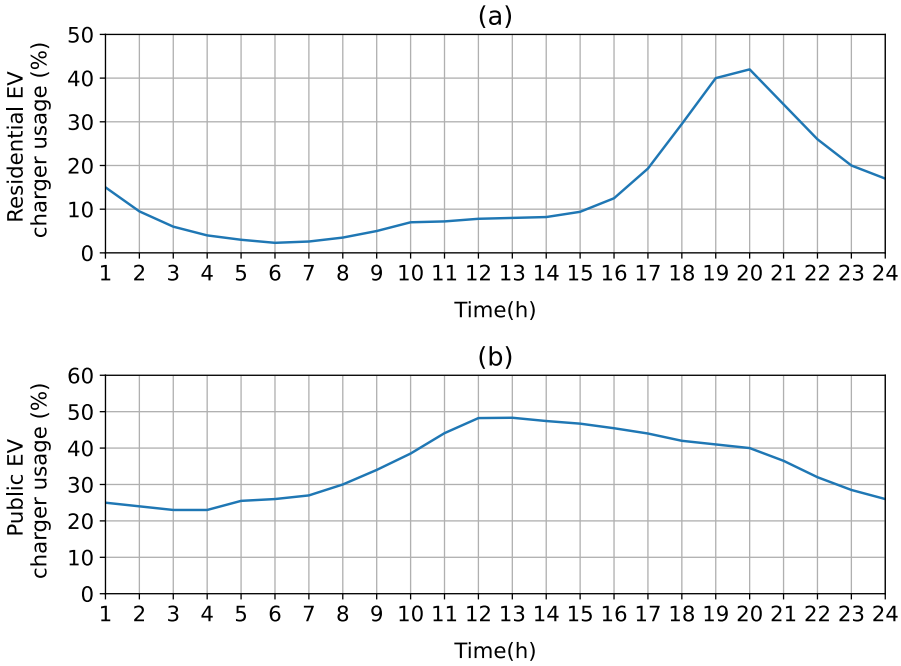

FIGURE 5. EV charging patterns, (a): residential EVCs [33], (b): public EVCs [34].

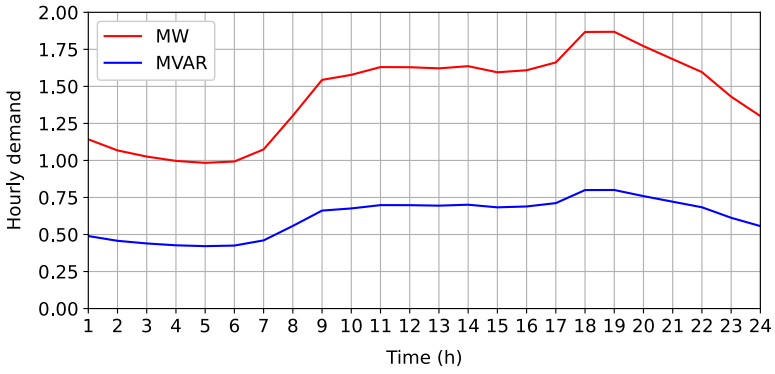

FIGURE 6. Hourly grid demand.

that in the baseline EVCs' profiles, the residential EVCs' demand is primarily increased during the early night hours. On the other hand, as shown in Fig. 5-(b), public EVCs are mainly demanded during the daytime. The grid's demand profile has shown in Fig. 6. The grid's demand is modeled as ZIP model for both active and reactive power. The demand is specified to be 20% constant complex power, 40% constant impedance, and 40% constant current. Considering the grid's demand profile shown in Fig. 6, these EVCs demand behavior forces more stress on the current electricity grid since the EVCs' demand is added during the system peak interval. Also, it should be noted that the load model for the EVCs' is considered constant current. Moreover, both EVCs have a power factor of 0.9.

Integration of RESs such as PVs (the most common type of RESs in distribution levels) can significantly affect the EVCs profile. However, EVCs' energy consumption can raise the energy injection through PVs since the operational obstacles, such as voltage rise and feeder thermal limits, can be alleviated. In this paper, each PV unit is considered to produce 2 kW with a power factor of 0.9. The PVs profile data is adopted from the UK database for the interval of 1/1/2020 to 26/6/2020 [35]. Also, The PV profile is depicted in Fig. 7. As well as EVCs', the PVs are modeled as constant current loads.

Eventually, it should be noticed that in both scenarios, 1000 × 2 kW PVs, 1000 × 3.7 kW residential EVCs, and 20 × 4 × 22 kW public EVCs are optimally located and

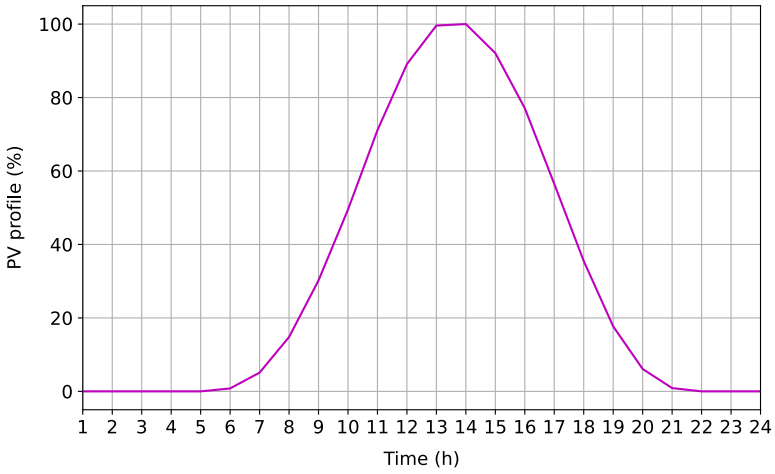

FIGURE 7. Hourly PV profile.

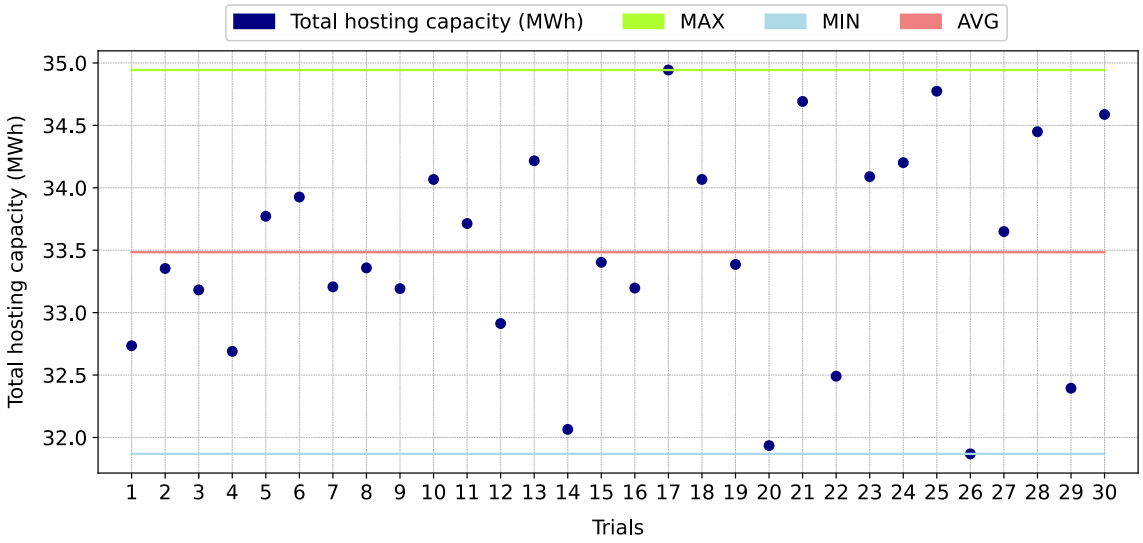

FIGURE 8. Results of trials in scenario-I (without considering VRs).

installed at load points. Moreover, at each load point, two units of PVs and residential EVCs can be installed simultaneously, where six units of public EVCs can be installed at each load point.

In the second scenario, a sensitivity analysis was conducted for several VRs. Also, their location and reference voltages will be chosen optimally.

D. SCENARIO-I: INCREASING THE HC FOR PVs AND BOTH EVCs WITHOUT CONSIDERING VRs

This scenario aims to increase the HC for PVs and EVCs without considering VRs by optimally locating the PVs and EVCs and their generated or consumed reactive power. The TVAC-IPSO algorithm will find the best locations for PVs and EVCs in the LV grid and their generated or consumed reactive power. Best found locations and reactive powers have been evaluated by 24-hour power flow in the given grid. For this scenario, 30 separate trials have been done, and the best solutions are depicted in Fig. 8.

According to Fig. 8, the best solutions for the total HC have resulted by optimally locating the PVs and EVCs. It is worth noticing that the total nominal power that can be installed in the grid is around 42.352 MWh. Maximum total HC was found in the 17th trial, about 34.943 MWh. The average total HC of all 30 trials is about 33.484 MWh. Also, in Table 2, the number of EVCs and PVs units connected to all LV feeders in the 17th trial can be seen, where 85.7% of PVs, 80.2% of residential EVCs, and 81.25% of public EVCs are installed.

E. SCENARIO-II: INCREASING HC FOR PVs AND BOTH EVCs, CONSIDERING VRs

In this scenario, the HC for PVs and EVCs will be observed by adding VRs to the point that the LV feeder is connected to the MV grid. The locations of the VRs will be found

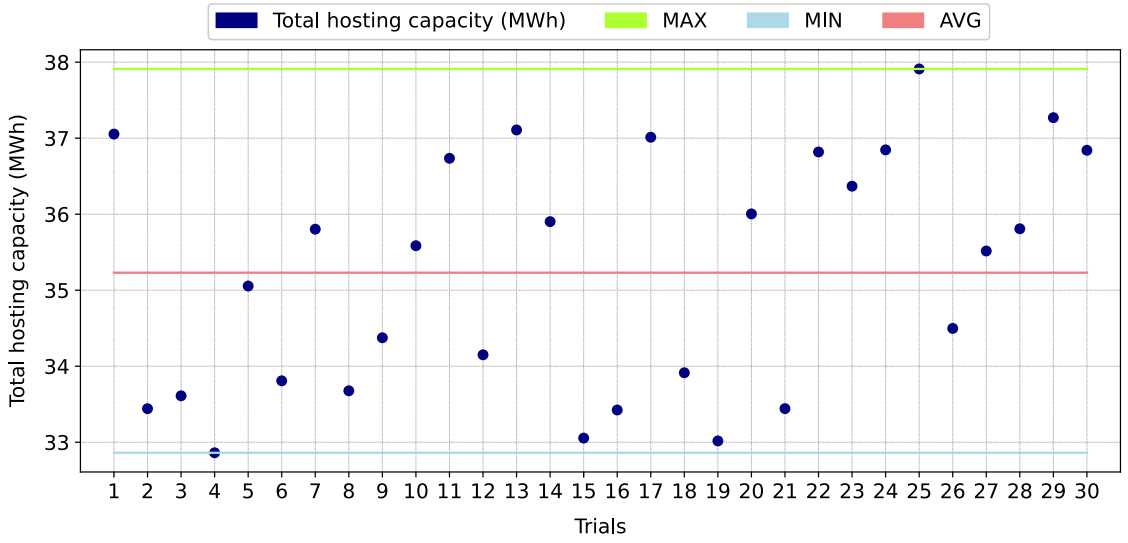

FIGURE 9. Results of trials in scenario-II using 1 VR.

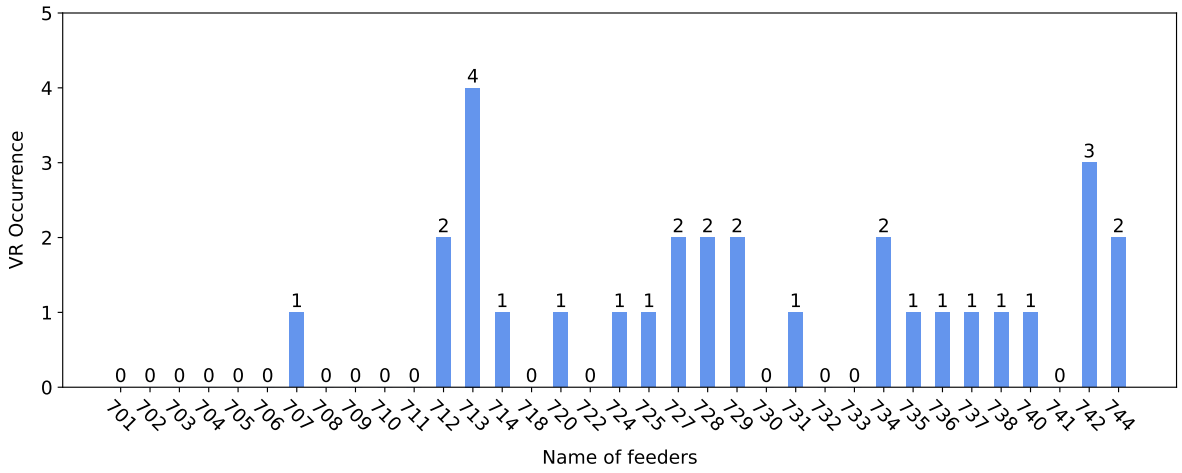

FIGURE 10. VR occurrence of scenario-II trials using 1 VR.

TABLE 2. Number of EVCs and PVs units connected to all LV feeders in the 17th trial of scenario-I trials.

	PV	Residential EVC	Public EVC	Total
Installed units	857	802	65[1]	1724

[1] Out of 80 ($20 \times 4 = 80$).

optimally by the TVAC-IPSO algorithm, as well as the reference voltages of VRs. Thus, there will be 30 trials for each 1, 2, 3, and 4 VRs connected to LV feeders. Furthermore, the reference voltages of each phase of VR can be chosen separately. Best found locations for EVCs and PVs and their generated or consumed reactive power, optimal locations of VRs and reference voltages have been evaluated by 24-hour power flow in the given grid.

As the first step, 1 VR is added to the grid. The best solutions for 30 trials are depicted in Fig. 9. According to Fig. 9, the maximum total HC was found in the 25th trial, about 37.911 MWh. The HC's average value of trials with 1 VR is 1.746 MWh more than the HC's average value of trials in scenario-I. Also, the location of VR and its reference voltages for the 25th trial is shown in Table 3. Moreover, in Table 4, the number of EVCs and PV units connected to all LV feeders in the 25th trial using 1 VR can be seen. 98.3% PVs, 96.3% residential EVCs, and 75% public EVCs are installed. More 282 units of the mentioned DERs are installed, compared to the results of scenario-I in Table 2, showing the effectiveness of installing VR in improving the HC. In Fig. 10, feeders that VRs are connected in 30 trials are shown with their occurrence.

In the second step, 2 VRs will be connected to the grid. According to Fig. 11, the maximum total HC among 30 trials resulted in the 13th trial, around 38.761 MWh. The average value of all these best found solutions is about 35.627 MWh, 0.397 MWh more than the average value of 1 VR best

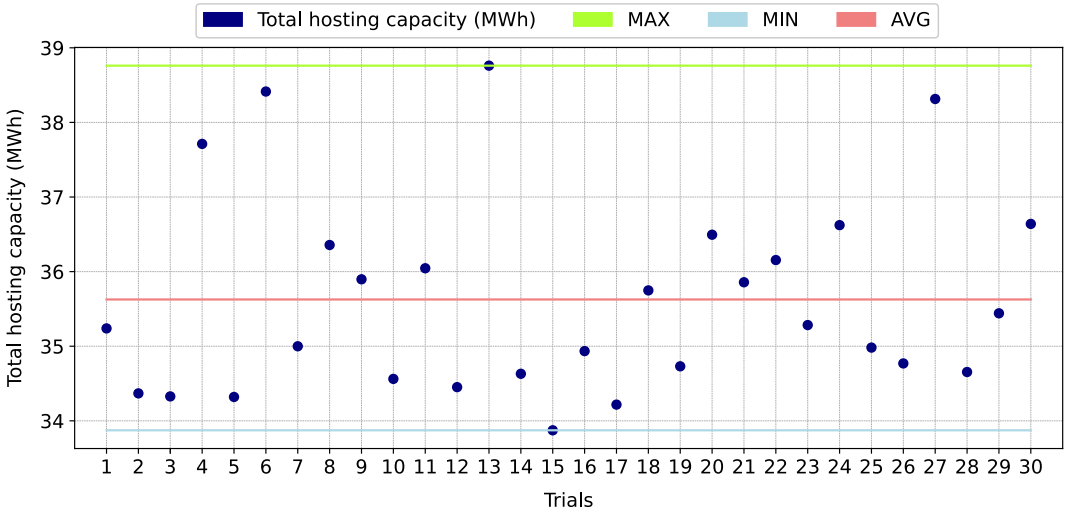

FIGURE 11. Results of trials in scenario-II using 2 VRs.

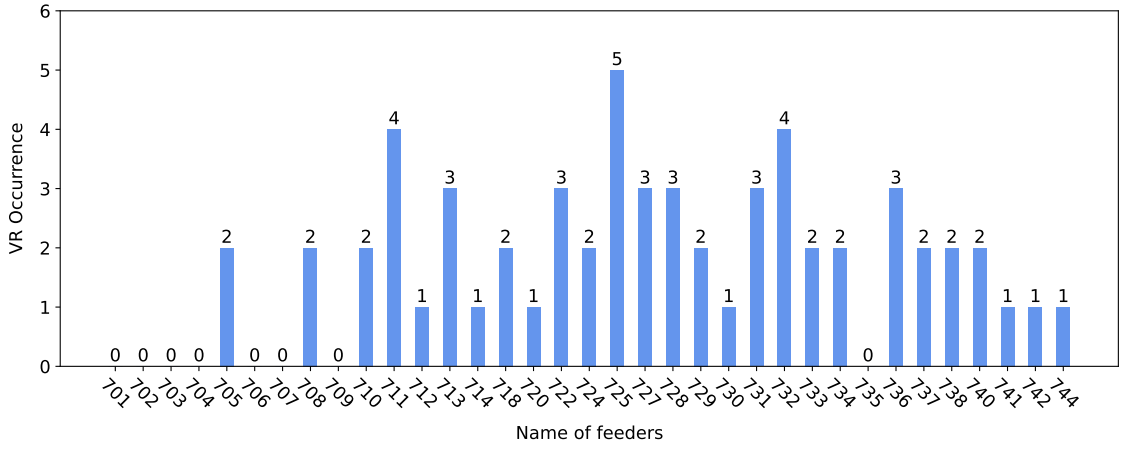

FIGURE 12. VR occurrence of scenario-II trials using 2 VRs.

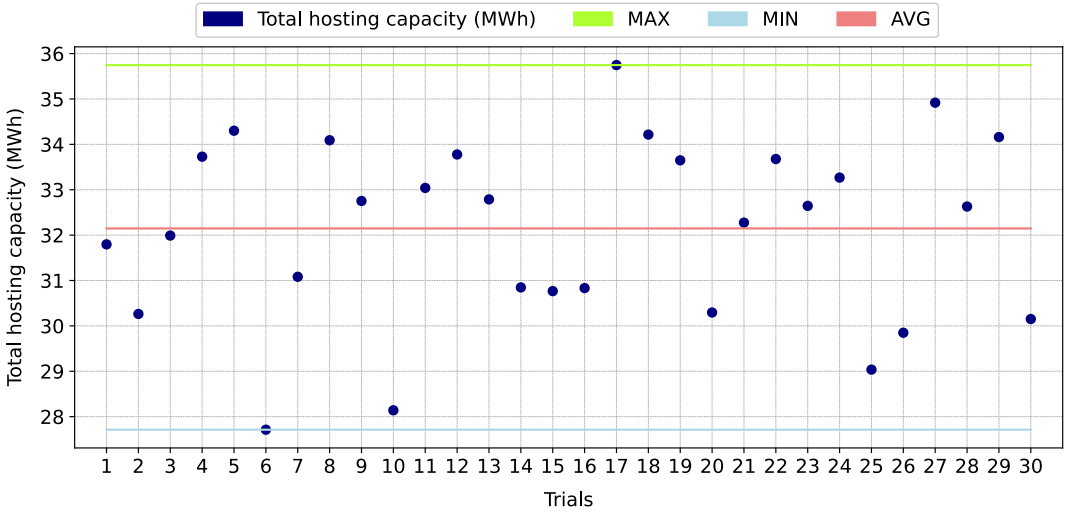

FIGURE 13. Results of trials in scenario-II using 3 VRs.

solution and 2.143 MWh more than the best solution found in scenario-I. The locations of 2 VRs and their reference voltages for the 13th trial are shown in Table 5. The number of EVCs and PV units connected to all LV feeders in the 13th trial is depicted in Table 6. According to Table 6, 994 units of PVs, 988 units of residential EVCs, and 62 units of public

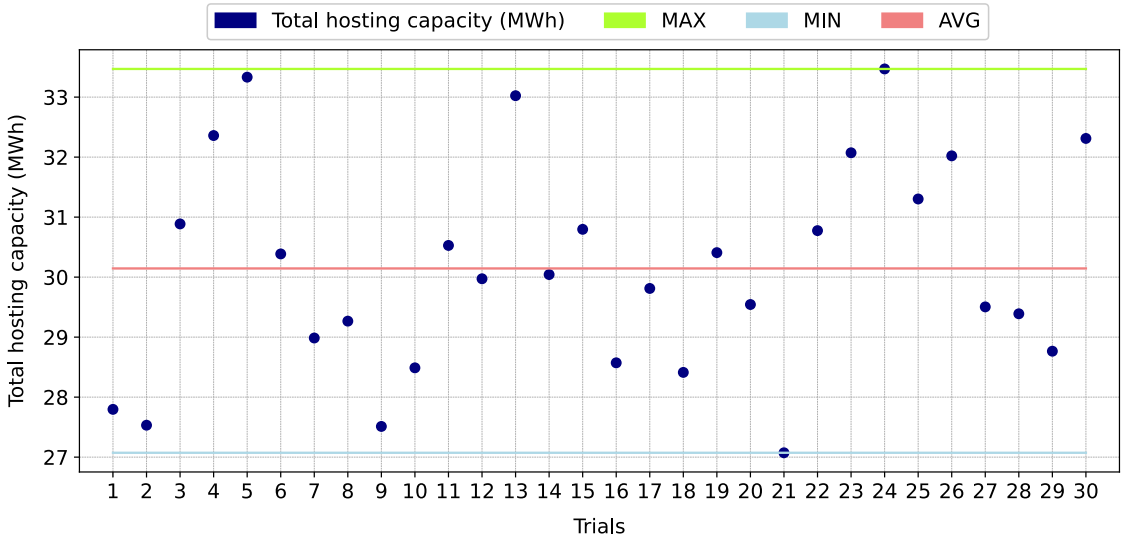

FIGURE 14. Results of trials in scenario-II using 4 VRs.

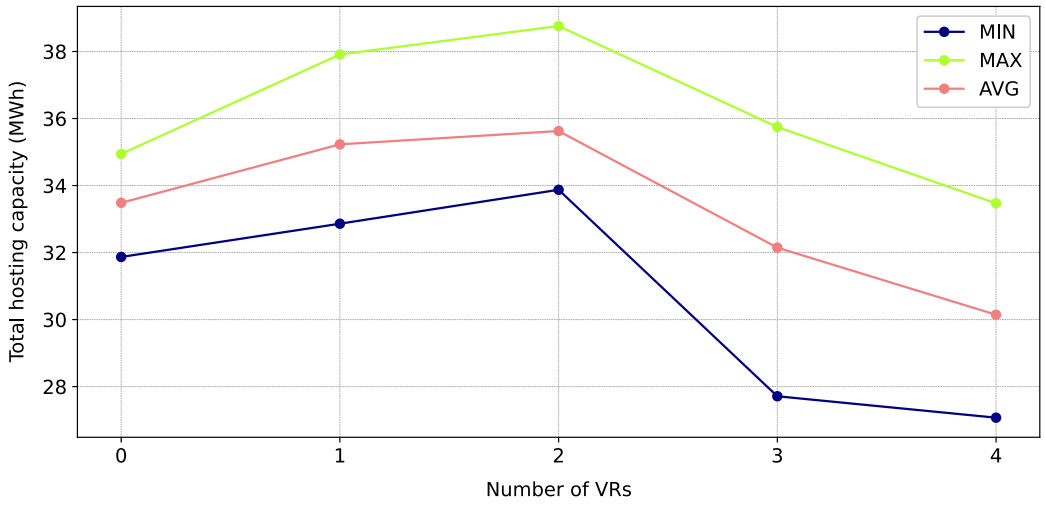

FIGURE 15. Relationship between numbers of VRs and HC.

TABLE 3. Location of VR and its reference voltages in 25th trial.

Name of feeder	Phase A	Phase B	Phase C
742	1.094	1.019	1

TABLE 4. Number of EVCs and PVs units connected to all LV feeders in the 25th trial of scenario-II trials using 1 VR.

	PV	Residential EVC	Public EVC	Total
Installed units	983	963	60[1]	2006

[1] Out of 80 ($20 \times 4 = 80$).

EVCs are installed. More 320 and 38 units of the mentioned DERs are installed, compared to the results of scenario-I in Table 2 and results of the test case with 1 VR in Table 4, respectively. In the second step, VR occurrence connecting to each feeder is shown in Fig. 12.

TABLE 5. Locations of 2 VRs and their reference voltages in 13th trial.

Name of feeders	Phase A	Phase B	Phase C
737	1.1	1.031	1.063
725	1.1	0.994	1

In the last step, 3 and 4 VRs are connected to the grid. As it can be seen from Fig. 13, the maximum best solution among 30 trials when 3 VRs are connected is in the 17th trial, that is about 35.747 MWh, and when 4 VRs are connected, the maximum best solution is in the 24th trial, which is about

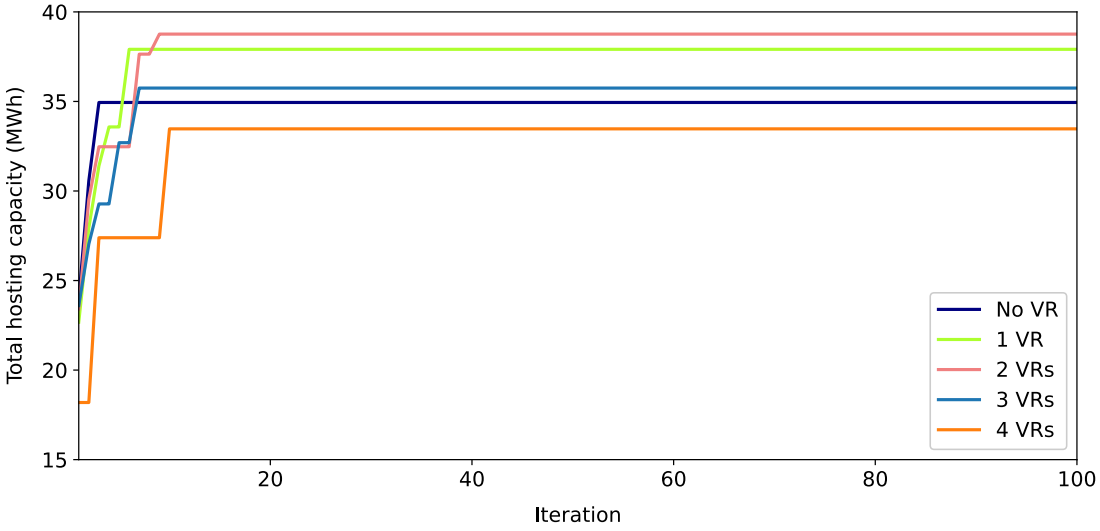

FIGURE 16. Convergence characteristics of the proposed algorithm in different test cases.

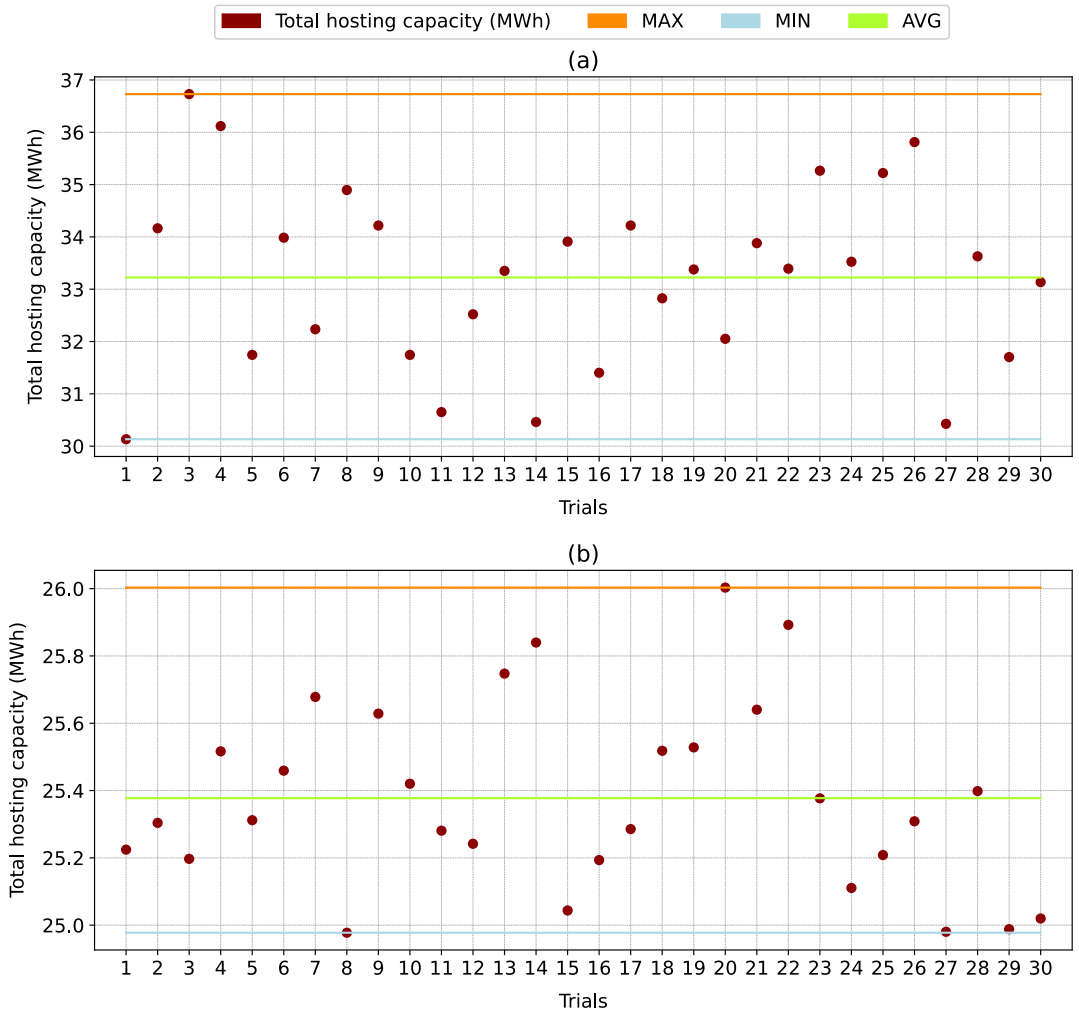

FIGURE 17. Results of trials using 2 VRs implemented by, (a): PSO, (b): GA.

33.469 MWh that can be seen in Fig. 14. Considering the average values of the trials for both 3 and 4 VRs is apparent that by connecting 3 and 4 VRs to the grid, the HC decreases to 32.147 MWh and 30.145 MWh, respectively. Locations of

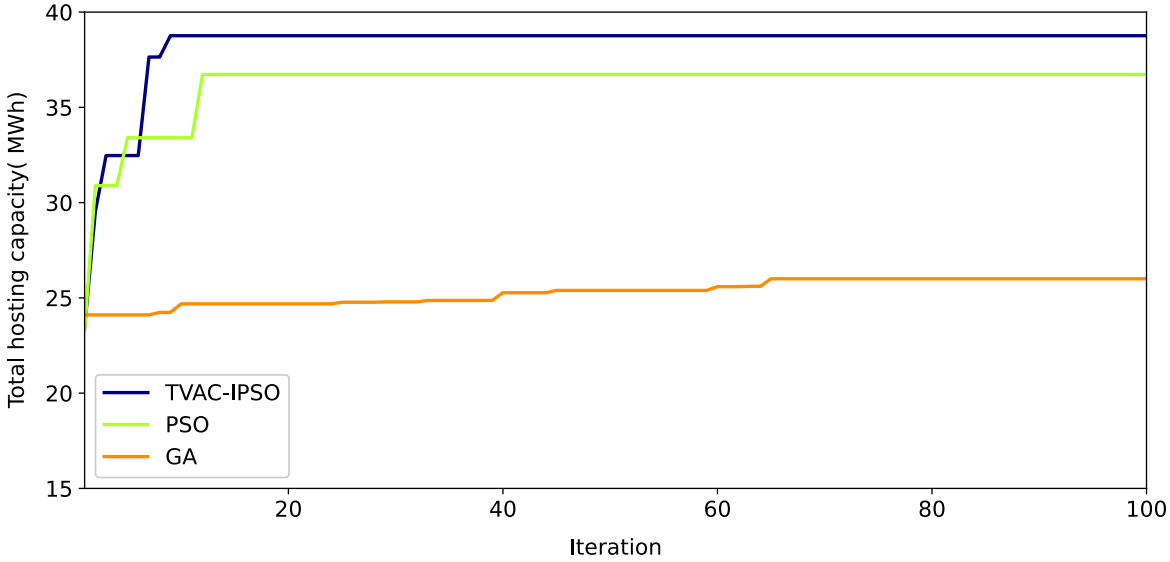

FIGURE 18. Convergence characteristics comparison of TVAC-IPSO, PSO, and GA.

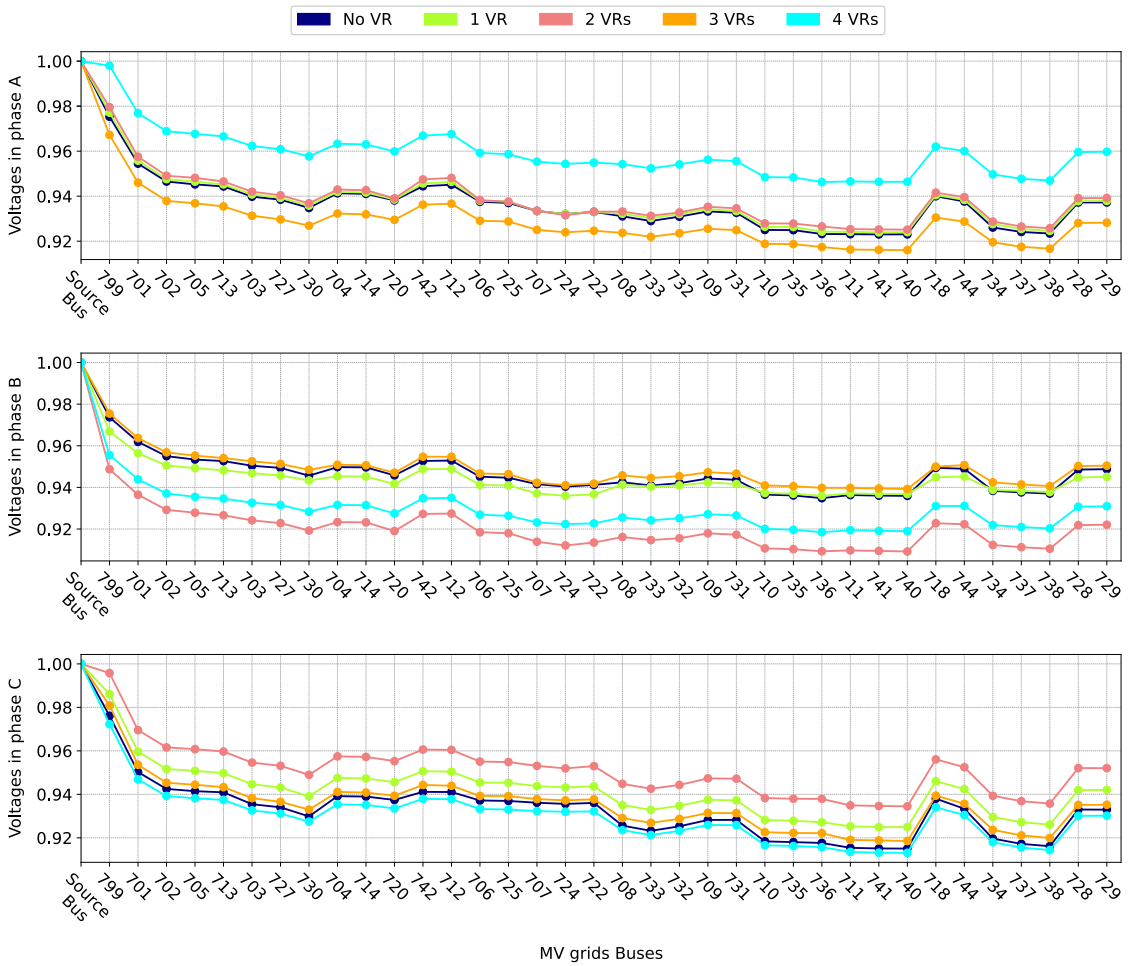

FIGURE 19. Voltages of each phase of buses in the MV grid at hour 19.

VRs and their reference voltages for best solutions in all cases in scenario-II are compared in Table 7.

According to Fig. 15, connecting 1 and 2 VRs increase the HC for EVCs and PVs, and connecting 2 VRs has the

TABLE 6. Number of EVCs and PVs units connected to all LV feeders in the 13th trial of scenario-II trials using 2 VRs.

	PV	Residential EVC	Public EVC	Total
Installed units	994	988	62[1]	2044

[1] Out of 80 ($20 \times 4 = 80$).

TABLE 7. Locations of VRs and their reference voltages in all cases of scenario-II.

Case	Name of feeders	Phase A	Phase B	Phase C
1 VR	742	1.094	1.019	1
2 VRs	737	1.1	1.031	1.063
	725	1.1	0.994	1
3 VRs	709	1.063	0.975	1.007
	722	1.019	1.063	0.963
	728	1.088	0.975	1.094
4 VRs	725	1.081	1.044	0.975
	732	0.963	0.975	1.019
	730	1.069	1.075	0.981
	728	1.088	1.088	1.019

most average value of the HC that resulted among scenarios, 35.627 MWh. However, by adding 3 and 4 VRs to the grid, HC starts to decrease to 30.145 MWh when 4 VRs are connected. This trend is all the same for the minimum and maximum results. In Fig. 16, the convergence characteristics of trials, which are the best solutions found in 30 trials of each case in scenario-I and scenario-II, have been shown. According to Fig. 16, all the trials converged before the 10th iteration, which proves that the proposed method has excellent performance.

Additionally, to prove the proposed method's optimal functionality, PSO and GA with 100 iterations and 50 particles and chromosomes in 30 trials have been conducted. All the trials were conducted for the case in which 2 VRs chose to be the optimal number of VRs. The mentioned results of trials for both algorithms are depicted in Fig. 17. Also, in Fig. 18, the convergence characteristics of the best solutions of PSO and GA, which are the 3rd and 20th, respectively, are compared to the best solution of the proposed method. As in Fig. 18, the PSO and GA algorithms suffer from premature convergence with equal given parameters compared to the proposed method, which also shows the better functionality of TVAC-IPSO method.

Increasing HC and adding VRs to the grid will affect the voltage profile of the grid. In Fig. 19, voltage profiles of each phase of all MV busses have been depicted. Voltage profiles have been chosen from the best solutions among all cases of both scenarios. All the depicted voltages are related to hour 19, the peak load hour.

IV. CONCLUSION

In this paper, an optimization model was proposed to determine the locations of large-scale penetration of public and residential EVCs and PVs, as well as their generated or consumed reactive power, optimal locations of VRs, and reference voltages to achieve the network's maximum HC for the DERs mentioned. Two scenarios were considered to compare the impact of the VRs on the HC of the network. The proposed model was implemented on the modified IEEE 37-node unbalanced MV distribution network connected to 35 real three-phase unbalanced LV distribution networks. Moreover, solving the problem using TVAC-IPSO helped to deal with the complicated optimization problem and avoid any violation of the system limits. Furthermore, several numbers of VRs were studied to obtain a suitable number of VRs for the case study. The results demonstrated that there was direct relevancy between the number of VRs and HC, as follows.

- By connecting two units of VRs, the HC was maximized, which was the optimal number of VRs in this study.
- When three and four VRs were connected, the HC decreased to its minimum values. In other words, with these numbers of VRs, the HC tended to decrease.

Therefore, the optimization model results showed that by connecting the optimal number of VRs to the grid and finding their optimal locations and reference voltages, the network's HC for EVCs and PVs can be increased.

REFERENCES

[1] IEA (2022). *Global EV Outlook 2022 Analysis IEA*. [Online]. Available: https://www.iea.org/reports/global-ev-outlook-2022
[2] I. Lampropoulos, T. Alskaif, W. Schram, E. Bontekoe, S. Coccato, and W. van Sark, "Review of energy in the built environment," *Smart Cities*, vol. 3, no. 2, pp. 248–288, Apr. 2020, doi: 10.3390/smartcities3020015.
[3] A. K. Jain, K. Horowitz, F. Ding, N. Gensollen, B. Mather, and B. Palmintier, "Quasi-static time-series PV hosting capacity methodology and metrics," in *Proc. IEEE Power Energy Soc. Innov. Smart Grid Technol. Conf. (ISGT)*, Feb. 2019, pp. 1–5, doi: 10.1109/ISGT.2019.8791569.
[4] R. Torquato, D. Salles, C. Oriente Pereira, P. C. M. Meira, and W. Freitas, "A comprehensive assessment of PV hosting capacity on low-voltage distribution systems," *IEEE Trans. Power Del.*, vol. 33, no. 2, pp. 1002–1012, Apr. 2018, doi: 10.1109/TPWRD.2018.2798707.
[5] A. Tavakoli, S. Saha, M. T. Arif, M. E. Haque, N. Mendis, and A. M. T. Oo, "Impacts of grid integration of solar PV and electric vehicle on grid stability, power quality and energy economics: A review," *IET Energy Syst. Integr.*, vol. 2, no. 3, pp. 243–260, Sep. 2020, doi: 10.1049/iet-esi.2019.0047.
[6] M. H. J. Bollen and F. Hassan, *Integration of Distributed Generation in the Power System*. Hoboken, NJ, USA: Wiley, 2011.
[7] S. I. Taheri, M. B. C. Salles, and A. B. Nassif, "Distributed energy resource placement considering hosting capacity by combining teaching–learning-based and honey-bee-mating optimisation algorithms," *Appl. Soft Comput.*, vol. 113, Dec. 2021, Art. no. 107953.
[8] T. Abbasi-Khazaei and M. H. Rezvani, "Energy-aware and carbon-efficient VM placement optimization in cloud datacenters using evolutionary computing methods," *Soft Comput.*, vol. 26, no. 18, pp. 9287–9322, Sep. 2022, doi: 10.1007/s00500-022-07245-y.
[9] A. S. Abbas, A. A. A. El-Ela, R. A. El-Sehiemy, and K. K. Fetyan, "Assessment and enhancement of uncertain renewable energy hosting capacity With/out voltage control devices in distribution grids," *IEEE Syst. J.*, early access, Jul. 13, 2022, doi: 10.1109/JSYST.2022.3180779.
[10] M. Alanazi, M. Mahoor, and A. Khodaei, "Co-optimization generation and transmission planning for maximizing large-scale solar PV integration," *Int. J. Electr. Power Energy Syst.*, vol. 118, Jun. 2020, Art. no. 105723, doi: 10.1016/j.ijepes.2019.105723.
[11] S. Arif, A. E. Rabbi, S. U. Ahmed, M. S. H. Lipu, T. Jamal, T. Aziz, M. R. Sarker, A. Riaz, T. Alharbi, and M. M. Hussain, "Enhancement of solar PV hosting capacity in a remote industrial microgrid: A methodical techno-economic approach," *Sustainability*, vol. 14, no. 14, p. 8921, Jul. 2022, doi: 10.3390/su14148921.

[12] E. Karunarathne, A. Wijethunge, and J. Ekanayake, "Enhancing PV hosting capacity using voltage control and employing dynamic line rating," *Energies*, vol. 15, no. 1, p. 134, Dec. 2021, doi: 10.3390/en15010134.
[13] D. Chathurangi, U. Jayatunga, S. Perera, A. P. Agalgaonkar, and T. Siyambalapitiya, "Comparative evaluation of solar PV hosting capacity enhancement using volt-VAr and volt-watt control strategies," *Renew. Energy*, vol. 177, pp. 1063–1075, Nov. 2021, doi: 10.1016/j.renene.2021.06.037.
[14] Y. Yao, F. Ding, K. Horowitz, and A. Jain, "Coordinated inverter control to increase dynamic PV hosting capacity: A real-time optimal power flow approach," *IEEE Syst. J.*, vol. 16, no. 2, pp. 1933–1944, Jun. 2022, doi: 10.1109/JSYST.2021.3071998.
[15] E. Vega-Fuentes and M. Denai, "Enhanced electric vehicle integration in the U.K. low-voltage networks with distributed phase shifting control," *IEEE Access*, vol. 7, pp. 46796–46807, 2019, doi: 10.1109/ACCESS.2019.2909990.
[16] R. Fachrizal, U. H. Ramadhani, J. Munkhammar, and J. Widén, "Combined PV–EV hosting capacity assessment for a residential LV distribution grid with smart EV charging and PV curtailment," *Sustain. Energy, Grids Netw.*, vol. 26, Jun. 2021, Art. no. 100445, doi: 10.1016/j.segan.2021.100445.
[17] E. C. da Silva, O. D. Melgar-Dominguez, and R. Romero, "Simultaneous distributed generation and electric vehicles hosting capacity assessment in electric distribution systems," *IEEE Access*, vol. 9, pp. 110927–110939, 2021, doi: 10.1109/ACCESS.2021.3102684.
[18] K.-S. Ryu, D.-J. Kim, H. Ko, C.-J. Boo, J. Kim, Y.-G. Jin, and H.-C. Kim, "MPC based energy management system for hosting capacity of PVs and customer load with EV in stand-alone microgrids," *Energies*, vol. 14, no. 13, p. 4041, Jul. 2021, doi: 10.3390/en14134041.
[19] R. Yang and Y. Zhang, "Three-phase AC optimal power flow based distribution locational marginal price," in *Proc. IEEE Power Energy Soc. Innov. Smart Grid Technol. Conf. (ISGT)*, Apr. 2017, pp. 1–5, doi: 10.1109/ISGT.2017.8086032.
[20] R. C. Dugan and T. E. McDermott, "An open source platform for collaborating on smart grid research," in *Proc. IEEE Power Energy Soc. Gen. Meeting*, Jul. 2011, pp. 1–7, doi: 10.1109/PES.2011.6039829.
[21] W. H. Kersting, "Distribution system modeling and analysis," in *Electric Power Generation, Transmission, and Distribution: The Electric Power Engineering Handbook*, 4th ed. Boca Raton, FL, USA: CRC Press, 2017.
[22] J. Kennedy and R. Eberhart, "Particle swarm optimization," in *Proc. IEEE Int. Conf. Neural Netw.*, vol. 4, Nov. 1995, pp. 1942–1948, doi: 10.1109/ICNN.1995.488968.
[23] J. Meng, H. G. Wang, Z. Dong, and K. P. Wong, "Quantum-inspired particle swarm optimization for valve-point economic load dispatch," *IEEE Trans. Power Syst.*, vol. 25, no. 1, pp. 215–222, Feb. 2010, doi: 10.1109/TPWRS.2009.2030359.
[24] K. T. Chaturvedi, M. Pandit, and L. Srivastava, "Self-organizing hierarchical particle swarm optimization for nonconvex economic dispatch," *IEEE Trans. Power Syst.*, vol. 23, no. 3, pp. 1079–1087, Aug. 2008, doi: 10.1109/TPWRS.2008.926455.
[25] A. Ratnaweera, S. K. Halgamuge, and H. C. Watson, "Self-organizing hierarchical particle swarm optimizer with time-varying acceleration coefficients," *IEEE Trans. Evol. Comput.*, vol. 8, no. 3, pp. 240–255, Jun. 2004, doi: 10.1109/TEVC.2004.826071.
[26] J.-B. Park, K.-S. Lee, J.-R. Shin, and K. Y. Lee, "A particle swarm optimization for economic dispatch with nonsmooth cost functions," *IEEE Trans. Power Syst.*, vol. 20, no. 1, pp. 34–42, Feb. 2005, doi: 10.1109/TPWRS.2004.831275.
[27] A. Safari and H. Shayeghi, "Iteration particle swarm optimization procedure for economic load dispatch with generator constraints," *Expert Syst. Appl.*, vol. 38, no. 5, pp. 6043–6048, May 2011, doi: 10.1016/j.eswa.2010.11.015.
[28] T.-Y. Lee and C.-L. Chen, "Unit commitment with probabilistic reserve: An IPSO approach," *Energy Convers. Manage.*, vol. 48, no. 2, pp. 486–493, 2007, doi: 10.1016/j.enconman.2006.06.015.
[29] T. Y. Lee, "Operating schedule of battery energy storage system in a time-of-use rate industrial user with wind turbine generators: A multipass iteration particle swarm optimization approach," *IEEE Trans. Energy Convers.*, vol. 22, no. 3, pp. 774–782, Sep. 2007, doi: 10.1109/TEC.2006.878239.
[30] K. T. Chaturvedi, M. Pandit, and L. Srivastava, "Particle swarm optimization with time varying acceleration coefficients for non-convex economic power dispatch," *Int. J. Electr. Power Energy Syst.*, vol. 31, no. 6, pp. 249–257, Jul. 2009, doi: 10.1016/j.ijepes.2009.01.010.
[31] *OpenDSS Open Distribution System Simulator*, EPRI, Washington, DC, USA, 2004.
[32] ENWL. *Low Voltage Network Solutions*. Accessed: Jul. 1, 2020. [Online]. Available: https://www.enwl.co.uk/go-net-zero/innovation/smaller-projects/low-carbon-networks-fund/low-voltage-network-solutions/
[33] T. Dodson and S. Slater, *Electric Vehicle Charging Behaviour Study: Final Report for National Grid ESO*. Menlo Park, CA, USA: Element Energy Limited, 2019.
[34] F. Pallonetto, M. Galvani, A. Torti, and S. Vantini, "A framework for analysis and expansion of public charging infrastructure under fast penetration of electric vehicles," *World Electr. Vehicle J.*, vol. 11, no. 1, p. 18, Feb. 2020, doi: 10.3390/wevj11010018.
[35] *National Grid*. Accessed: Jul. 1, 2020. [Online]. Available: https://www.nationalgrid.com/

SINA TOGHRANEGAR received the B.Sc. degree in electrical engineering and the M.Sc. degree in electrical power systems engineering from the University of Zanjan, Zanjan, Iran, in 2020 and 2022, respectively. His research interests include energy systems, power system operation and optimization, renewable energy systems, optimization of distribution networks, and low-carbon distribution networks.

ABBAS RABIEE (Senior Member, IEEE) received the Ph.D. degree in electrical engineering from Sharif University of Technology, Tehran, Iran, in 2013. He is currently an Associate Professor with the Department of Electrical and Electronic Engineering, University of Zanjan, Zanjan, Iran. His research interests include power system operation, renewable energies, integrated energy systems, and optimization methods. He was a recipient of the 2019 Premium Award for Best Paper in *IET Generation, Transmission & Distribution*.

SEYED MASOUD MOHSENI-BONAB (Senior Member, IEEE) received the Ph.D. degree from Université Laval, Québec, Canada, in 2020. He has been a Research Scientist with the Hydro-Quebec Research Institute (IREQ), since 2019, specializing in operation, security, and economy of power systems and smart grids, along with integrating renewable energy resources and optimization methods. He is an Adjunct Professor with Université Laval. He was a recipient of the 2019 Premium Award in *IET Generation, Transmission & Distribution*.